SCIENCE CHINA
Information Sciences

• RESEARCH PAPER •

April 2025, Vol. 68, Iss. 4, 140406:1–140406:10
https://doi.org/10.1007/s11432-024-4200-5

Special Topic: Photonics Technology

# Ultra-low power $MoS_2$ optoelectronic synapse with wavelength sensitivity for color target recognition

Bo WEI[1,2†], Yabo CHEN[1†], Xiaotong HAN[1], Yan KANG[3], Bujia LIANG[2], Cheng LI[4*], Xiaokuo YANG[2*], Liang FANG[1] & Yuanxi PENG[5*]

[1]*Institute for Quantum Information & State Key Laboratory of High Performance Computing, College of Computer, National University of Defense Technology, Changsha 410073, China*
[2]*Fundamentals Department, Air Force Engineering University, Xi'an 710051, China*
[3]*College of Advanced Interdisciplinary Studies, National University of Defense Technology, Changsha 410073, China*
[4]*Institute of Quantum Information Science and Technology, College of Science, National University of Defense Technology, Changsha 410073, China*
[5]*College of Computer, National University of Defense Technology, Changsha 410073, China*

Received 10 July 2024/Revised 4 August 2024/Accepted 22 October 2024/Published online 4 March 2025

**Abstract** Optoelectronic synapses that integrate visual perception and pre-processing hold significant potential for neuromorphic vision systems (NVSs). However, due to a lack of wavelength sensitivity, existing NVS mainly focuses on gray-scale image processing, making it challenging to recognize color images. Additionally, the high power consumption of optoelectronic synapses, compared to the 10 fJ energy consumption of biological synapses, limits their broader application. To address these challenges, an energy-efficient NVS capable of color target recognition in a noisy environment was developed, utilizing a $MoS_2$ optoelectronic synapse with wavelength sensitivity. Benefiting from the distinct photon capture capabilities of 450, 535, and 650 nm light, the optoelectronic synapse exhibits wavelength-dependent synaptic plasticity, including excitatory postsynaptic current (EPSC), paired-pulse facilitation (PPF), and long-term plasticity (LTP). These properties can effectively mimic the visual memory and color discrimination functions of the human vision system. Results demonstrate that the NVS, based on $MoS_2$ optoelectronic synapses, can eliminate the color noise at the sensor level, increasing color image recognition accuracy from 50% to 90%. Importantly, the optoelectronic synapse operates at a low voltage spike of 0.0005 V, consuming only 0.075 fJ per spike, surpassing the energy efficiency of both existing optoelectronic and biological synapses. This ultra-low power, color-sensitive device eliminates the need for color filters and offers great promise for future deployment in filter-free NVS.

**Keywords** optoelectronic synapse, neuromorphic vision system, color recognition, 2D materials, image pre-processing

**Citation** Wei B, Chen Y B, Han X T, et al. Ultra-low power $MoS_2$ optoelectronic synapse with wavelength sensitivity for color target recognition. Sci China Inf Sci, 2025, 68(4): 140406, https://doi.org/10.1007/s11432-024-4200-5

## 1 Introduction

With the continuous expansion of the exploration fields, artificial intelligence urgently requires more powerful artificial vision systems to perform brain-like tasks, such as motion detection, color recognition, and image denoising in extreme environments [1]. Traditional artificial vision systems generally consist of three main modules: a perception unit that receives optical stimuli and converts them into electrical signals, a storage unit that stores light information, and a processing unit that handles signal processing tasks [2]. However, these systems are limited by the physical separation of their sensing, storing, and processing units, leading to high redundancy and latency, which hampers their ability to efficiently perform complex brain-like tasks. This challenge significantly limits the potential of real-time video analysis, automatic driving, drone navigation, and purely visual robots. Notably, approximately 80% of the knowledge in the human brain is acquired through the human vision system (HVS), which can achieve visual perception with low redundancy, latency, and energy consumption [3, 4]. Inspired by the HVS, neuromorphic vision systems (NVS) that monolithically integrate sensing, storing, and processing functions have been proposed as alternatives to conventional artificial vision systems [5–9].

* Corresponding author (email: cheng.li@nudt.edu.cn, yangxk0123@163.com, pyx@nudt.edu.cn)
† Wei B and Chen Y B have the same contribution to this work.

 

The NVS can directly respond to light stimuli and mimic visual learning and memory through the short-term plasticity (STP) or long-term plasticity (LTP) of optoelectronic synapses. Such an all-in-one bionic device reduces energy consumption and improves efficiency. Currently, the synaptic plasticity of optoelectronic synapses has been demonstrated using nanowires, perovskites, and two-dimensional materials [10–12]. NVS constructed from these optoelectronic synapses exhibits various vision-like functions, including polarization-sensitive visual adaption, multimode perception, and multi-target recognition [13–16]. However, due to limitations in the photosensitive layer, these optoelectronic synapses are not adaptive to light wavelength, making them incapable of distinguishing different colors from the real world, let alone mimicking the color pattern recognition of the human vision system. The ability of optoelectronic synapses to recognize color is crucial for NVS, as it enhances the perception capability of robots. Some studies have color discrimination capabilities, but they are either limited to a three-terminal structure or suffer from high power consumption [17–20]. Therefore, the development of simplified optoelectronic synapses that can spontaneously distinguish colors in an energy-efficient manner will pave the way for advanced NVS. Recently, molybdenum disulfide ($MoS_2$), a typical two-dimensional semiconductor material, has been widely reported as a key material for optoelectronic synapses due to its large absorption cross-section, wide bandgap, and high thermal stability [21–24]. Devices based on $MoS_2$ can simulate a variety of biological synaptic behaviors, such as STP, LTP, and paired-pulse facilitation (PPF). Considering $MoS_2$'s broad absorption across the entire visible spectrum, this material exhibits the potential to mimic the color recognition ability of the human vision system.

Here, we demonstrate a gate-free two-terminal $MoS_2$ optoelectronic synapse. The distinguishable photoconductive effect of this device enables it to exhibit different synaptic plasticities depending on the light wavelength. Based on these results, our device can distinguish three colors (red, blue, and green) at the sensor level. Consequently, an NVS constructed with an array of these optoelectronic synapses can perform feature extraction from mix-colored patterns by reducing redundant data. Furthermore, this optoelectronic synapse array can filter background noise, mimicking the image pre-processing function. The pre-processed image recognition rate of the Modified National Institute of Standards and Technology (MNIST) handwritten dataset was significantly improved from 50% to 90%. Additionally, synaptic plasticity remained apparent when the reading voltage was set to 0.0005 V, with the calculated power consumption being 0.075 fJ per spike. In particular, this optoelectronic synapse is compared with other devices reported heretofore, in terms of light wavelength, power consumption, and device architecture. The device integrates light perception, storage, and pre-processing functions into a simple, gate-free, two-terminal architecture, offering a new approach to developing energy-efficient, color-sensitive NVSs with low redundancy and latency. This technology shows great potential for future application in automatic driving and intelligent robotics.

## 2 Results and discussion

The retina plays a significant role in color discrimination, image recognition, and motion detection, relying on various photoreceptors (rods and cones), neurons, and synapses. When optical stimuli reach the photoreceptors through the cornea and crystalline lens, they are absorbed by rods and cones, generating electrical impulses. These pulses are transferred to the retina's neural network for storing and pre-processing, where features such as color, brightness, and speed of moving objects are extracted and encoded. The retina's high efficiency in classifying unstructured data is driven by the synaptic plasticity of its synapses, including both STP and LTP. These critical features can be integrated into an all-in-one neuromorphic imaging device known as the optoelectronic synapse. This device can respond directly to light stimuli, exhibiting light-triggered synaptic plasticity similar to synaptic functions in the retina. The efficiency of this neuromorphic imaging device, compared to conventional imaging systems, is illustrated in Figure S1. Traditional artificial vision systems rely on separate modules for sensing, storing, and pre-processing vast amounts of optical data, which results in significant redundancy and latency. These systems often require an image sensors array, storage device, and CPU, working independently to capture, store, and process massive light information, leading to time delays and accumulation of redundant data. In contrast, NVS built by optoelectronic synapses beat traditional vision system in acquisition and recognition efficiency, reducing latency while improving performance. Figures 1(a) and (b) present a schematic comparison between the human retina and a gate-free, two-terminal optoelectronic synapse that simulates the photoreceptors and synapse functions. This device, fabricated using two-dimensional

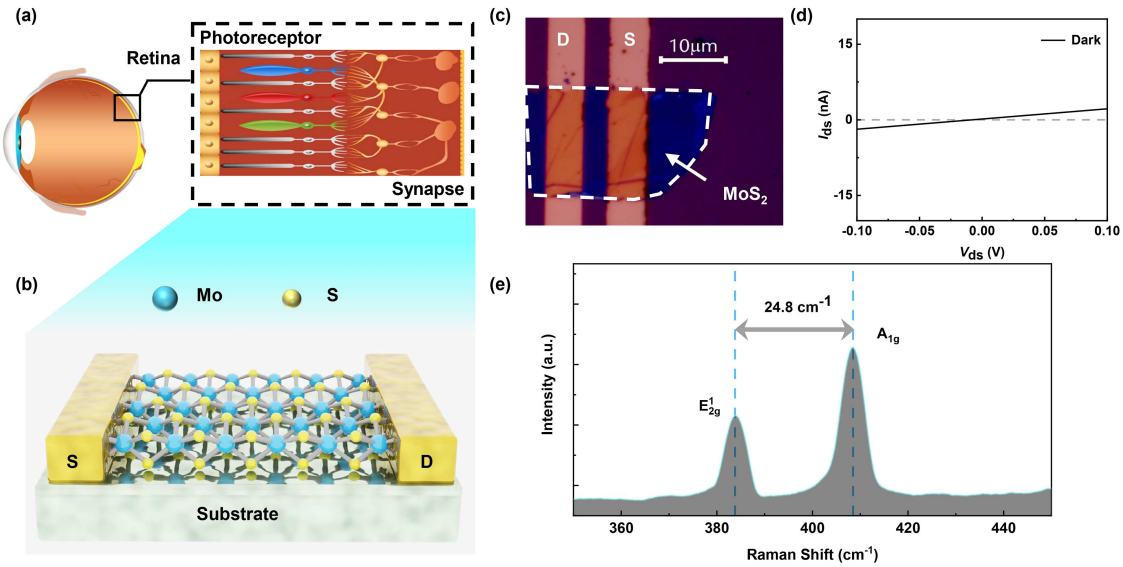


**Figure 1** (Color online) Retina and characterization of two-terminal $MoS_2$ optoelectronic synapses. (a) The retina adapting to incident light with different spectral compositions through different photoreceptors (red, blue, green) and realizing image memory, feature extraction, and motion detection based on synapses; (b) schematic diagram of a gate-free two-terminal optoelectronic synapse made from $MoS_2$; (c) optical microscope image of the optoelectronic synapse; (d) output characteristics in the dark environment, $V_{ds}$ varying from −0.1 to 0.1 V; (e) Raman spectroscopy of $MoS_2$ thin film.

$MoS_2$ prepared on a $Si/SiO_2$ substrate, employs molybdenum disulfide as the channel layer to transmit photocurrent. The D and S represent the drain and source electrodes, respectively. Figure 1(c) shows an optical microscope image of the device's top view, with dashed areas indicating multilayer $MoS_2$. Light acts as the presynaptic stimulus, while the drain-source electrode serves as the postsynaptic terminal, accumulating excitatory postsynaptic current (EPSC). Figure 1(d) demonstrates the device's output characteristic curve under a swept drain-source voltage from −0.1 to 0.1 V, showing a linear relationship between current and voltage. The linearity suggests an Ohmic contact between the $MoS_2$ channel and Au electrodes. The Raman spectrum in Figure 1(e) further confirms the multilayer property of the $MoS_2$ thin film.

To explore the device's optical responses, a 650 nm light stimulus (red) was applied, and the change of ΔEPSC was measured at a constant $V_{ds} = 0.1$ V unless otherwise specified. The exposure to light causes a sudden increase in ΔEPSC, followed by a gradual decay after light removal, as shown in Figures 2(a)–(c). The slow decay of ΔEPSC after 650 nm exposure is attributed to the persistent photoconductivity (PPC) effect of $MoS_2$, which is essential for mimicking light-induced synaptic plasticity and memory-like behaviors. Figures 2(a) and (b) demonstrate that the duration time and intensity of light stimulus significantly affect the ΔEPSC decay trend, highlighting a light-controlled transition from STP to LTP. Additionally, The device's adaptability was tested by decreasing the operating voltage, as shown in Figure 2(c). Remarkably, the optoelectronic synapse maintains significant synaptic plasticity even at a low voltage, suggesting that the power consumption can be minimized by applying a low voltage. In conditions of weak light, increasing the operating voltage can enhance photocurrent, demonstrating the device's environmentally resilient. In Figure 2(d), the device exhibits varying levels of ΔEPSC in response to light stimuli of different intensities and duration time. Similar to the retina, the device generates a higher ΔEPSC for brighter and longer-appearing targets. To further analyze the transition from STP to LTP induced by light, the memory retention of ΔEPSC ($I_{MR}$) is calculated as follows:

$$I_{MR} = (I_t - I_{off})/(I_{max} - I_{off}), \tag{1}$$

where $I_t$ denotes the EPSC after $t$ s, $I_{off}$ is the initial current, and $I_{max}$ is the maximum EPSC. The ΔEPSC decay process can be fitted with Kohlraush stretched-exponential function [25]:

$$I_{MR} = \exp\left[-\left(\frac{t}{\tau}\right)^{\beta}\right], \tag{2}$$

where $\tau$ denotes the decay time constant, representing the non-volatile characteristic, and $\beta$ is the stretch

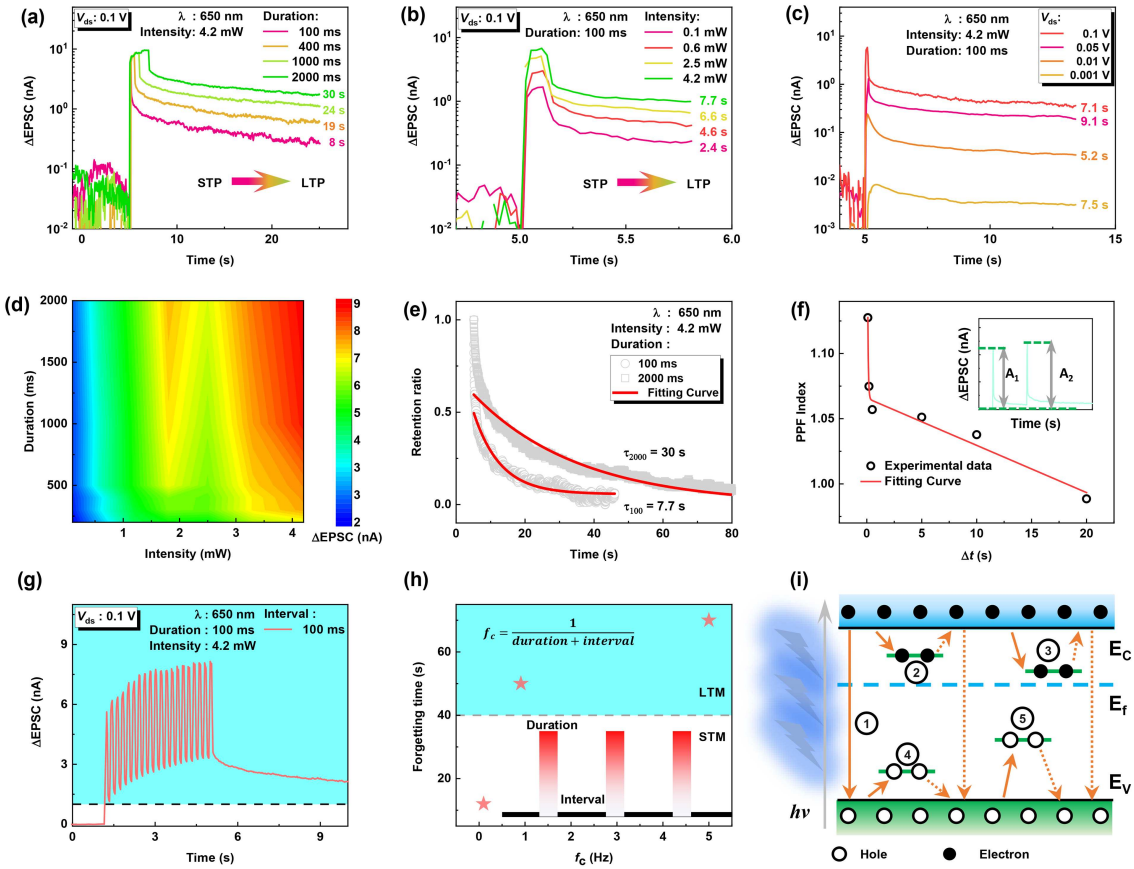


**Figure 2** (Color online) Synaptic plasticity of $MoS_2$ optoelectronic synapse. Optical responses under (a) different light duration time, (b) different light intensity, and (c) different reading voltage. (d) The heatmap of ΔEPSC triggered at different light stimuli in terms of light intensity and duration time. (e) The experimental data and fitting curve of memory retention ratio. (f) PPF index versus interval time $\Delta t$ and the fitting curve. The inset shows ΔEPSC triggered by two consecutive light pulses, definitions of $\Delta t$, $A_1$, and $A_2$. (g) ΔEPSC measured by 20 red light pulses with intensity = 4.2 mW, duration time = 100 ms, and interval time = 100 ms. A current threshold = 1 nA is set to evaluate the device's memory effect. (h) Transition from STM to LTM under different frequencies. The frequency is varied by increasing the interval time of the optical pulses, while keeping the duration time fixed. (i) Band model of $MoS_2$ under optical illumination. The blue dotted line represents the Fermi energy, and the green dotted line represents the impurity energy level.

index. Figure 2(e) exhibits two synaptic plasticities (STP and LTP) when the duration time of the light stimuli is 100 and 2000 ms, respectively. Longer duration time means higher ΔEPSC; therefore, longer decay time is required (high $\tau$). In other words, longer vision memory can be obtained. The light stimuli act as a presynaptic spike and the photocurrent acts as the postsynaptic current. Subsequently, two consecutive light pulses were tested on this device. As shown in the inset of Figure 2(f), the ΔEPSC generated by the second light pulse is higher than the first, like a relay race. This behavior is very similar to the PPF of biological synapses, implying that our device can serve as a light-controlled optoelectronic synapse. The PPF index can be quantitatively described as

$$\text{PPF index} = \frac{A_2}{A_1} \times 100\%, \tag{3}$$

where $A_1$ and $A_2$ denote the ΔEPSC induced by the first and the second light pulse, respectively. Figure 2(f) describes the PPF index as a function of light pulse interval time $\Delta t$. The experimental results show that the PPF index decreases from 112% to 98%, implying a potential of mimicking biological synapses. The PPF index curve can be fitted by the following formula [26]:

$$Y = 1 + C_1 \exp\left(-\frac{\Delta t}{\tau_1}\right) + C_2 \exp\left(-\frac{\Delta t}{\tau_2}\right), \tag{4}$$

where $C_1$ and $C_2$ represent the initial facilitation magnitude, and $\tau_1$, $\tau_2$ denote the characteristic relaxation times for the rapid and slow decay terms, respectively. Specifically, $\tau_1$ (54 ms) corresponds to the fast

relation process, while $\tau_2$ (1362 ms) represents the slow relaxation process. The distinctions between the rapid and slow decay terms, as well as the associated time constants, are analog to those found in biological synapses [27].

The synaptic weights of the optoelectronic synapses can be monotonically modulated by multiple presynaptic spikes, a mechanism essential for accumulating and transmitting information within neural networks. Furthermore, vision memory and image recognition in the retina also involve the interaction of multiple input spikes. To investigate synaptic plasticity in the proposed optoelectronic synapse stimulated by multiple spikes, 20 repeated light pulses were applied to assess the accumulation of ΔEPSC. In Figure 2(g), red light pulses (light intensity: 4.2 mW, duration time: 100 ms, interval time: 100 ms, pulse number: 20) are employed as presynaptic spikes, with the corresponding ΔEPSC plotted. The 20 repeated light pulses result in a higher ΔEPSC compared to a single light stimulus, attributed to the consolidation of synaptic plasticity. To evaluate light-induced memory, a current threshold of 1 nA is set, and the short-term memory (STM) and long-term memory (LTM) behavior of the optoelectronic synapse is examined by analyzing the forgetting time (i.e., the time required for ΔEPSC to decay to the threshold). In Figure 2(h), an increasing trend in forgetting time with respect to light frequency is observed. A lower frequency (e.g., 0.099 Hz) induces STM, while a high frequency (e.g., 5 Hz) triggers LTM. This LTM-STM behavior is attributed to the illumination time-dependent variation in ΔEPSC within $MoS_2$ optoelectronic synapse. This STM-to-LTM conversion process mimics the memory model of the human brain, specifically the "learning-forgetting-relearning" cycle, as illustrated in Figure S2. Optical inputs received with attention (learning) are initially converted to STM, which is stored for a brief period (a few seconds). If the frequent reinforcement (relearning) occurs, STM is transferred to LTM, which may last for several minutes. As with human learning behavior, the more frequent the external light pulse, the better the memory retention in the optoelectronic synapses. Longer intervals between stimuli may result in STM or even memory loss. These results suggest that synaptic plasticity is closely associated with the frequency of stimulation. The origin of PPC in $MoS_2$, along with its dependence on illumination time and light intensity, can be explained by a band model based on trap states, as shown in Figure 2(i). Midgap trap states in $MoS_2$ originate from defects, surface adsorbates, or interfacial imperfections, which are inevitable during the growth of multilayer $MoS_2$ and the device fabrication process. Light excites electrons from the valence band ($E_V$) to the conduction band ($E_C$). Following excitation, electrons in $E_C$ can directly recombine with holes in $E_V$ (①). However, some electrons are trapped (②: shallow trap, ③: deep trap) and require thermal excitation to reach $E_C$ before recombining with holes in $E_V$. Similarly, trapped holes (④: shallow trap, ⑤: deep trap) also require thermal excitation to reach $E_V$ and recombine with electrons. These trapped carriers inside $MoS_2$ delay the recombination of photo-generated carriers, which is responsible for the observed PPC effect in this device. This behavior is consistent with previous reports on $MoS_2$ optoelectronic synapses [25, 28–31].

One crucial ability of the retina is color discrimination, allowing it to extract key objects from a mixed-colored noisy environment, similar to the process involved in color blindness tests. Utilizing a color recognition mechanism to extract key information can effectively reduce interference caused by redundant data, thus improving the speed of subsequent image processing steps. To mimic the retina's color-discrimination ability, different light stimuli (red, blue, and green) were applied to the $MoS_2$ optoelectronic synapse. The dependence of ΔEPSC on light color was investigated later (Figures 3(a) and (b)). The distinguishable ΔEPSC value can be attributed to differences in the optical absorption coefficients of photons with varying wavelengths [32]. In Figures 3(a) and (b), the optoelectronic synapse exhibits wavelength-sensitive synaptic plasticity (STP, LTP, and the transition process from STP to LTP). This wavelength-selective optical response characteristic endows the device with the capability for color discrimination. Based on this wavelength selection characteristic, we simulated an NVS constructed using an array of optoelectronic synapses and investigated the vision memory effect of color targets. In Figure 3(c), red "H," green "O," and blue "T" were illuminated on a $3 \times 3$ sensor array. The color pixels represent a series of 30 light pulses (intensity: 4.7 mW, duration time: 100 ms, interval time: 100 ms), while black pixels indicate no light excitation. Figure 3(d) shows the change in ΔEPSC at 0, 10, and 30 s after the light is turned off. After an extended period, the blue "T" still retains a high ΔEPSC, while the green "O" and red "H" gradually fade. These results suggest that the NVS based on the optoelectronic synapse exhibits color-dependent memory, with both STM and LTM, and transitions between the two. In the human vision system, STM and LTM play a significant role in filtering redundant noisy data and extracting features from mix-colored patterns. Figure 3(e) presents a schematic diagram of the feature extraction process in the human vision system. The retina does not merely sense the image information

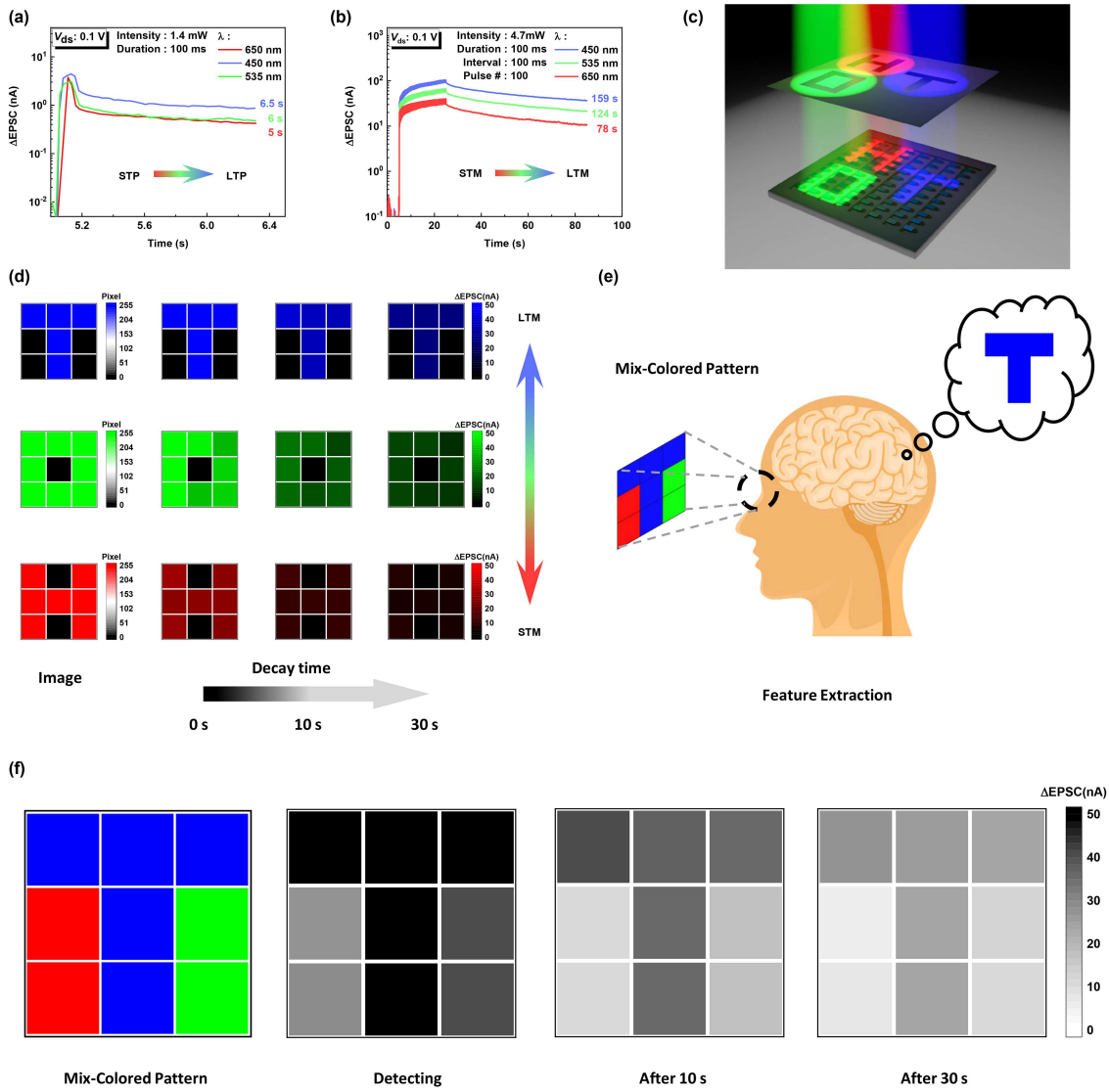


**Figure 3** (Color online) Vision memory and mix-colored pattern recognition in NVS mimicking the human vision system. (a) ΔEPSC triggered by 450, 535, 650 nm light stimuli. (b) ΔEPSC triggered by 450, 535, and 650 nm light pulses. (c) Schematic diagram of NVS constructed by a 3 × 3 optoelectronic synapses array. Red 'H', green 'O', and blue 'T' are illuminated to NVS, respectively. (d) The change of ΔEPSC at 0, 10, and 30 s after the light is turned off. In the color image, the colored pixels represent a series of 30 light pulses (intensity: 4.7 mW, duration time: 100 ms, interval time: 100 ms) with 650 nm (bottom), 535 nm (middle), 450 nm (top) applied to NVS while black pixels mean no light. (e) Schematic diagram of human vision system realizing feature extraction. (f) Mix-colored pattern recognition based on NVS by reducing redundant color information.

that falls upon it; rather, it extracts information from a noisy environment and sends it to the visual cortex. Thus, the blue "T" in the mix-colored pattern can be accurately recognized by the human vision system. In this color recognition process, the retina acts as both a sensor and a pre-processing unit. A similar intelligent behavior can be observed in the NVS constructed with this optoelectronic synapse, as shown in Figure 3(f). When a mix-colored image is perceived by the optoelectronic synapse, the light information is converted into ΔEPSC. However, due to its wavelength-sensitive memory, the red and green noise gradually fades, while the blue target becomes more apparent. Similar to the retina, the $MoS_2$ optoelectronic synapse achieves in-sensor preprocessing to filter redundant data. This integrated sensing and preprocessing capability significantly enhances image recognition efficiency and reduces the latency of the NVS.

Benefiting from the color recognition capability of the $MoS_2$ optoelectronic synapse, the extraction of the blue target in a real image can be demonstrated using the NVS. In Figure 4(a), the red (R), green (G), and blue (B) components were sampled before being fed into the NVS. The features of the balloon, background, and box were prominent in the R, G, and B images, respectively. The R, G, and

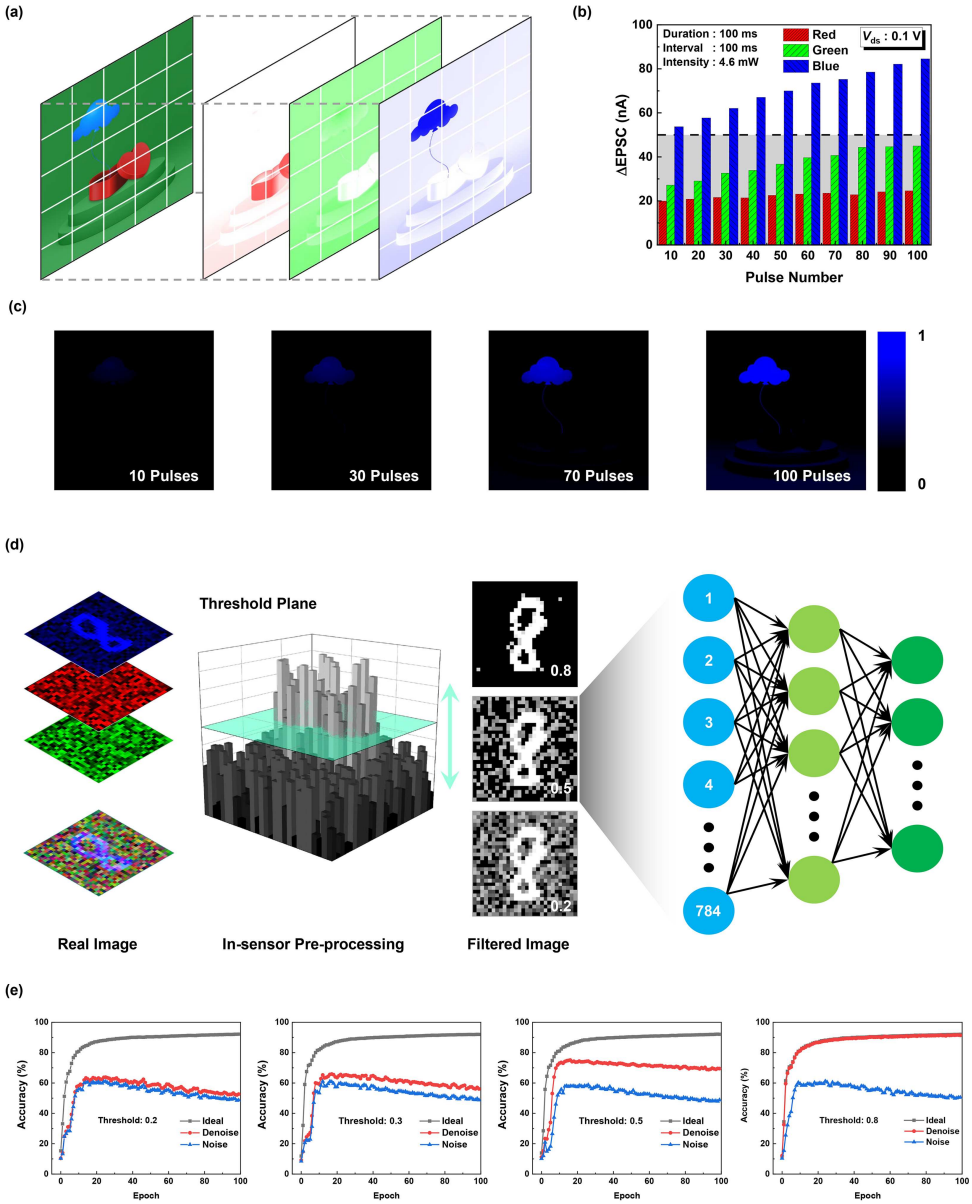


**Figure 4** (Color online) Color target recognition and image denoising by NVS. (a) Schematic diagram of encoding color information into light intensity; (b) statistical information on the relationship between ΔEPSC and pulse number; (c) color target recognition by increasing the contrast between blue and other targets; (d) image denoising in NVS and recognition in artificial neural network (ANN); (e) comparisons of the recognition accuracy on different datasets.

B values were then mapped to light intensities of 650, 535, and 450 nm, respectively. Accordingly, the relationship between light intensity and ΔEPSC is shown in Figure S3. The dependence of ΔEPSC on the number of light pulses (light intensity: 4.6 mW, duration time: 100 ms, interval time: 100 ms) is shown in Figure 4(b). The contrast between the blue target and other targets was enhanced with an increasing number of pulses. As a result, the blue balloon target became clearer in Figure 4(c). This occurs because the blue regions in the image produce higher ΔEPSC, and after normalizing the ΔEPSC of the optoelectronic synapse, only the blue regions remain noticeable. This result indicates that multiple pulses can continuously enhance the recognition of blue targets in the NVS, effectively distinguishing them from the original color image. When the retina recognizes a specific target in the environment, interference from other colors often occurs, which we define as redundant noise. In traditional artificial vision systems, filtering out these noises typically requires a large number of peripheral circuits, leading to inevitable issues such as data latency and power consumption. To explore the image-denoising capabilities of the NVS, an artificial neural network (ANN) was designed (Figure 4(d)), where the NVS serves as

**Table 1** Device structure and performance of optoelectronic synapses in literature.

| Ref. | Photosensing material | Structure | Wavelength (nm) | Energy consumption |
|---|---|---|---|---|
| [18] | P(VDF-TrFE)/$ReS_2$ | Top gate FET | 450, 530, 650 | 64 fJ |
| [29] | Monolayered $MoS_2$ | Back gate FET | 450, 532, 633 | 26.9 pJ |
| [30] | $TiN_xO_{2-x}/MoS_2$ | Two-terminal | 365 | 450 nJ |
| [32] | $MoS_2$/BTO | Back gate FET | 450, 530, 650 | 1.8 pJ |
| [34] | IGZO/$Al_2O_3$ | Back gate FET | 405 | 750 fJ |
| [35] | Perovskite/ITO/PEN | Two-terminal | 630 | 1.2 nJ |
| [36] | PQD-MWCNT | Two-terminal | 405 | 6.1 nJ |
| [37] | $Ti_3C_2T_x$/MXenes | Back gate FET | 365 | 100 fJ |
| [38] | Te | Back gate FET | 532 | 110 fJ |
| [39] | $MoS_2$/h-BN | Back gate FET | 365, 405 | 450 pJ |
| [40] | $CuInP_2S_6$/h-BN/$\alpha$-$In_2Se_3$ | Top gate FET | 532 | 250 pJ |
| [41] | $MoS_2/Hb_2O_5$ | Back gate FET | 532 | 6 pJ |
| [42] | $MoSe_2/Bi_2Se_3$ | Back gate FET | 790 | 140 nJ |
| [43] | Silicon nanocrystals | Back gate FET | 1342 | 9140 nJ |
| [44] | InGaAs | Back gate FET | 1550 | 0.675 fJ |
| [45] | IZGO | Back gate FET | 405 | 0.0845 fJ |
| [46] | $MoS_2$/DNTT | Two-terminal | 500, 600 | 0.4 fJ |
| [47] | IGZO | Two-terminal | 405 | 20 fJ |
| [48] | $In_2Se_3/MoS_2$ | Two-terminal | 1060 | 28 fJ |
| **This work** | **$MoS_2$** | **Two-terminal** | **450, 535, 650** | **0.075 fJ** |

the sensing and pre-processing unit to filter redundant noise data, and the ANN functions as the image recognition component to identify the processed image. The original MNIST handwritten digits (ideal), the MNIST dataset with R&G noise (noise), and the MNIST dataset pre-processed by the NVS (denoise) were used as inputs. In Figure 4(d), the real noisy image "8" is presented. The image was sampled into R, G, and B components. As mentioned above, when the NVS was fed with the R, G, and B images, the optical signal was converted into the $\Delta$EPSC of $MoS_2$ optoelectronic synapse and stored for an extended period. However, the blue areas excite higher $\Delta$EPSC, as shown in the second inset of Figure 4(d). Different image filtering effects are achieved by selecting different threshold planes, and the output filtered images were read from the $\Delta$EPSC of the optoelectronic synapses. The filtered image information was then normalized and sent to an ANN consisting of an input layer (784 nodes), a hidden layer (300 nodes), and an output layer (10 nodes) for image recognition. As shown in Figure 4(e), the recognition accuracy of the noise MNIST dataset only reached about 50% after 100 epochs, slightly higher than the initial accuracy, indicating that the ANN had difficulty recognizing such datasets. In contrast, the recognition accuracy on the ideal and denoised datasets was consistent, reaching about 90% after 100 epochs, which was significantly higher than the accuracy achieved before denoising. The image-denoising process undeniably influences recognition accuracy. As shown in the four illustrations in Figure 4(e), the recognition accuracy of the denoised datasets progressively increases. This result indicates that the in-sensor pre-processing capabilities of the NVS can effectively extract information, reduce redundant noise data, and enable accurate image recognition even on noisy color images.

NVS with color differentiation mechanisms show advantages over other artificial vision systems; however, high power consumption may negate these advantages. As a result, power consumption is a crucial factor in determining whether NVS will become a practical reality. The synaptic plasticity of the device under 0.0005 V is illustrated in Figure S4. The energy consumption is expressed as follows:

$$E = V_{\rm ds} \times I_{\rm peak} \times t_{\rm duration}, \tag{5}$$

where $I_{\rm peak}$ represents the peak EPSC through the channel, $t_{\rm duration}$ signifies the duration time of the light stimuli, and $V_{\rm ds}$ denotes the source-drain voltage. The minimum calculated energy consumption for a single light spike is 0.075 fJ, which is significantly lower than that of biological synapses and existing optoelectronic synapses [33]. These results indicate that this device has exceptionally low power consumption, making it suitable for use in extremely low-energy environments. It offers an appealing solution for future vision-based applications, such as autonomous driving and bionic eyes. Table 1 summarizes the performance of the proposed optoelectronic synapse bold in the table compared to previously reported studies [18, 29, 30, 32, 34–48], highlighting its superior applicability in future NVSs.

## 3 Conclusion

In summary, a gate-free, two-terminal optoelectronic synapse utilizing multilayer $MoS_2$ as a light-sensitive channel was developed. This optoelectronic synapse exhibits light-tunable synaptic plasticity, including EPSC, STP, LTP, and PPF. Furthermore, NVS based on this device can distinguish and retain color information while extracting important features from a noisy environment, much like the human retina. Image recognition tests using ANN revealed that the recognition accuracy on the MNIST handwritten datasets increased from 50% to 90% by filtering out redundant noise. The device's power consumption is calculated to be 0.075 fJ per spike, outperforming biological and existing optoelectronic synapses. This work demonstrates the potential for fabricating in-sensor pre-processing optoelectronic synapses for ultra-low power color recognition, offering promise for future advanced NVSs.

**Acknowledgements** This work was supported by National Natural Science Foundation of China (Grant Nos. 61832007, 62274183), Key Program of National Natural Science Foundation of China (Grant No. U22A2027), and National Key Research and Development Program of China (Grant No. 2023YFB4502100).

**Supporting information** Figures S1–S4. The supporting information is available online at info.scichina.com and link.springer.com. The supporting materials are published as submitted, without typesetting or editing. The responsibility for scientific accuracy and content remains entirely with the authors.

**References**

1 Zhou F, Chai Y. Near-sensor and in-sensor computing. Nat Electron, 2020, 3: 664–671
2 Zhou F, Zhou Z, Chen J, et al. Optoelectronic resistive random access memory for neuromorphic vision sensors. Nat Nanotechnol, 2019, 14: 776–782
3 Huang X, Li Q, Shi W, et al. Dual-mode learning of ambipolar synaptic phototransistor based on 2D perovskite/organic heterojunction for flexible color recognizable visual system. Small, 2021, 17: 2102820
4 Lee K, Han H, Kim Y, et al. Retina-inspired structurally tunable synaptic perovskite nanocones. Adv Funct Mater, 2021, 31: 2105596
5 Choi C, Leem J, Kim M, et al. Curved neuromorphic image sensor array using a $MoS_2$-organic heterostructure inspired by the human visual recognition system. Nat Commun, 2020, 11: 5934
6 Hou Y X, Li Y, Zhang Z C, et al. Large-scale and flexible optical synapses for neuromorphic computing and integrated visible information sensing memory processing. ACS Nano, 2020, 15: 1497–1508
7 Chen Y B, Huang Y J, Zeng J W, et al. Energy-efficient $ReS_2$-based optoelectronic synapse for 3D object reconstruction and recognition. ACS Appl Mater Interfaces, 2023, 15: 58631–58642
8 Li S Y, Li J T, Zhou K, et al. In-sensor neuromorphic computing using perovskites and transition metal dichalcogenides. J Phys Mater, 2024, 7: 032002
9 Lian H, Liao Q, Yang B, et al. Optoelectronic synaptic transistors based on upconverting nanoparticles. J Mater Chem C, 2021, 9: 640–648
10 Huang Z, Li Y, Zhang Y, et al. 2D multifunctional devices: from material preparation to device fabrication and neuromorphic applications. Int J Extrem Manuf, 2024, 6: 032003
11 Chen X, Chen B, Jiang B, et al. Nanowires for UV-vis-IR optoelectronic synaptic devices. Adv Funct Mater, 2023, 33: 2208807
12 Wang Y, Lv Z, Chen J, et al. Photonic synapses based on inorganic perovskite quantum dots for neuromorphic computing. Adv Mater, 2018, 30: 1802883
13 Kang Y, Chen Y, Tan Y, et al. Bioinspired activation of silent synapses in layered materials for extensible neuromorphic computing. J Materiomics, 2023, 9: 787–797
14 Xie D, Gao G, Tian B, et al. Porous metal-organic framework/$ReS_2$ heterojunction phototransistor for polarization-sensitive visual adaptation emulation. Adv Mater, 2023, 35: 2212118
15 Su J, Li Y, Xie D, et al. Vertical 0.6 V sub-10 nm oxide-homojunction transistor gated by a silk fibroin/sodium alginate crosslinking hydrogel for pain-sensitization enhancement emulation. Mater Horiz, 2023, 10: 1745–1756
16 Chen Y B, Kang Y, Hao H, et al. All two-dimensional integration-type optoelectronic synapse mimicking visual attention mechanism for multi-target recognition. Adv Funct Mater, 2023, 33: 2209781
17 Shao H, Li Y, Yang W, et al. A reconfigurable optoelectronic synaptic transistor with stable Zr-$CsPbI_3$ nanocrystals for visuomorphic computing. Adv Mater, 2023, 35: 2208497
18 Dang Z, Guo F, Zhao Y, et al. Ferroelectric modulation of $ReS_2$-based multifunctional optoelectronic neuromorphic devices for wavelength-selective artificial visual system. Adv Funct Mater, 2024, 34: 2400105
19 Ma F, Zhu Y, Xu Z, et al. Optoelectronic perovskite synapses for neuromorphic computing. Adv Funct Mater, 2020, 30: 1908901
20 Hu L, Yang J, Wang J, et al. All-optically controlled memristor for optoelectronic neuromorphic computing. Adv Funct Mater, 2021, 31: 2005582
21 Tran M D, Kim H, Kim J S, et al. Two-terminal multibit optical memory via van der Waals heterostructure. Adv Mater, 2019, 31: 1807075
22 Wang S, Chen C, Yu Z, et al. A $MoS_2$/PTCDA hybrid heterojunction synapse with efficient photoelectric dual modulation and versatility. Adv Mater, 2019, 31: 1806227
23 Cheng Y, Li H, Liu B, et al. Vertical 0D-perovskite/2D-$MoS_2$ van der Waals heterojunction phototransistor for emulating photoelectric-synergistically classical pavlovian conditioning and neural coding dynamics. Small, 2020, 16: 2005217
24 Xie D, Wei L, Xie M, et al. Photoelectric visual adaptation based on 0D-$CsPbBr_3$-quantum-dots/2D-$MoS_2$ mixed-dimensional heterojunction transistor. Adv Funct Mater, 2021, 31: 2010655
25 George A, Fistul M V, Gruenewald M, et al. Giant persistent photoconductivity in monolayer $MoS_2$ field-effect transistors. npj 2D Mater Appl, 2021, 5: 15
26 Li D, Li C, Ilyas N, et al. Color-recognizing Si-based photonic synapse for artificial visual system. Adv Intelligent Syst, 2020, 2: 2000107
27 Kwon S M, Cho S W, Kim M, et al. Environment-adaptable artificial visual perception behaviors using a light-adjustable optoelectronic neuromorphic device array. Adv Mater, 2019, 31: 1906433
28 Zhang W, Huang J K, Chen C H, et al. High-gain phototransistors based on a CVD $MoS_2$ Monolayer. Adv Mater, 2013, 25: 3456–3461

29 Huang M, Ali W, Yang L, et al. Multifunctional optoelectronic synapses based on arrayed $MoS_2$ monolayers emulating human association memory. Adv Sci, 2023, 10: 2300120
30 Wang W, Gao S, Li Y, et al. Artificial optoelectronic synapses based on $TiN_xO_{2-x}/MoS_2$ heterojunction for neuromorphic computing and visual system. Adv Funct Mater, 2021, 31: 2101201
31 Sahu M C, Sahoo S, Mallik S K, et al. Multifunctional 2D $MoS_2$ optoelectronic artificial synapse with integrated arithmetic and reconfigurable logic operations for in-memory neuromorphic computing applications. Adv Mater Technologies, 2023, 8: 2201125
32 Du J, Xie D, Zhang Q, et al. A robust neuromorphic vision sensor with optical control of ferroelectric switching. Nano Energy, 2021, 89: 106439
33 Zhang C, Wang S, Zhao X, et al. Sub-femtojoule-energy-consumption conformable synaptic transistors based on organic single-crystalline nanoribbons. Adv Funct Mater, 2021, 31: 2007894
34 Song S, Choi C, Ahn J, et al. Artificial optoelectronic synapse based on spatiotemporal irradiation to source-sharing circuitry of synaptic phototransistors. Infomat, 2024, 6: e12479
35 Cai B, Huang Y, Tang L, et al. All-optically controlled retinomorphic memristor for image processing and stabilization. Adv Funct Mater, 2023, 33: 2306272
36 Li J, Dwivedi P, Kumar K S, et al. Growing perovskite quantum dots on carbon nanotubes for neuromorphic optoelectronic computing. Adv Elect Mater, 2021, 7: 2000535
37 Zhao T, Zhao C, Xu W, et al. Bio-inspired photoelectric artificial synapse based on two-dimensional $Ti_3C_2T_x$ MXenes floating gate. Adv Funct Mater, 2021, 31: 2106000
38 Yoon J, You B, Kim Y, et al. Environmentally stable and reconfigurable ultralow-power two-dimensional tellurene synaptic transistor for neuromorphic edge computing. ACS Appl Mater Interfaces, 2023, 15: 18463–18472
39 Oh S, Lee J J, Seo S, et al. Photoelectroactive artificial synapse and its application to biosignal pattern recognition. npj 2D Mater Appl, 2021, 5: 95
40 Baek S, Yoo H H, Ju J H, et al. Ferroelectric field-effect-transistor integrated with ferroelectrics heterostructure. Adv Sci, 2022, 9: 2200566
41 Nam J H, Oh S, Jang H Y, et al. Low power $MoS_2/Nb_2O_5$ memtransistor device with highly reliable heterosynaptic plasticity. Adv Funct Mater, 2021, 31: 2104174
42 Wang Y, Yang J, Ye W, et al. Near-infrared-irradiation-mediated synaptic behavior from tunable charge-trapping dynamics. Adv Elect Mater, 2020, 6: 1900765
43 Yin L, Han C, Zhang Q, et al. Synaptic silicon-nanocrystal phototransistors for neuromorphic computing. Nano Energy, 2019, 63: 103859
44 Kim T S, Jeon S, Ko K, et al. Fast, energy-efficient InGaAs synaptic phototransistors on flexible substrate. Adv Elect Mater, 2023, 9: 2300437
45 Zhu L, Li S X, Lin J C, et al. Ultra-low power IGZO optoelectronic synaptic transistors for neuromorphic computing. Sci China Inf Sci, 2024, 67: 222401
46 Wang J, Yang B, Dai S, et al. Weak light-stimulated synaptic transistors based on $MoS_2$/organic semiconductor heterojunction for neuromorphic computing. Adv Mater Technologies, 2023, 8: 2300449
47 Zhu Y, Peng B, Zhu L, et al. IGZO nanofiber photoelectric neuromorphic transistors with indium ratio tuned synaptic plasticity. Appl Phys Lett, 2022, 121: 133502
48 Hu Y, Yang H, Huang J, et al. Flexible optical synapses based on $In_2Se_3/MoS_2$ heterojunctions for artificial vision systems in the near-infrared range. ACS Appl Mater Interfaces, 2022, 14: 55839–55849